A Fault Diagnosis Framework for Centrifugal Pumps by Scalogram-Based Imaging and Deep Learning

MD JUNAYED HASAN[1], **AKHAND RAI**[1,2], **ZAHOOR AHMAD**[1],
AND JONG-MYON KIM[1], **(Member, IEEE)**

[1]Department of Electrical, Electronics and Computer Engineering (BK21Four), University of Ulsan, Ulsan 44610, South Korea
[2]School of Engineering and Applied Sciences, Ahmedabad University, Ahmedabad 380009, India

Corresponding author: Jong-Myon Kim (jmkim07@ulsan.ac.kr)

ABSTRACT Centrifugal pumps are the most vital part of any process industry. A fault in centrifugal pump can affect imperative industrial processes. To ensure reliable operation of the centrifugal pump, this paper proposes a novel automated health state diagnosis framework for centrifugal pump that combines a signal to time-frequency imaging technique and an Adaptive Deep Convolution Neural Network model (ADCNN). First, the vibration signals corresponding to different health conditions of the centrifugal pump are acquired. Vibration signals obtained from the centrifugal pump carry a great deal of information and generally, statistical features are extracted from the vibration signals to retain meaningful fault information. However, these features are either insensitive to weak incipient faults or unsuitable for tracking severe faults, thus, decreasing the fault classification accuracy. To tackle this problem, a signal to time-frequency imaging technique is applied to the pump vibration signals. For this purpose, Continuous Wavelet Transform (CWT) is applied to decompose the vibration signals over different time-frequency scales and extract the pump fault information in both the time and frequency domains. The CWT scales form two-dimensional time-frequency images commonly referred to as scalograms. The CWT scalograms are then converted into grayscale images (SGI). Over the past few decades, CNN models have been established as an effective practice to process images for classification and pattern recognition. Consequently, the extracted CWTSGIs are finally provided as inputs to the proposed ADCNN architecture to achieve feature extraction and classification for centrifugal pump faults. The performance of the proposed diagnostic framework (CWTSGI + ADCNN) is validated with a vibration dataset collected from a testbed specifically designed for centrifugal pump diagnosis. The experimental results suggest that the proposed technique based on CWTSGI and ADCNN outperformed existing methods with an average performance improvement of 4.7 – 15.6%.

INDEX TERMS Centrifugal pump, continuous wavelet transformations, scalogram, gray images, convolutional neural network.

I. INTRODUCTION

Centrifugal pumps play a crucial role in many important engineering industries such as oil refineries, mining, and electric power plants, etc. [1]. The failure of centrifugal pumps causes an increase in process downtime, interruptions in operations, and hazardous accidents. This results in financial losses and sometimes leads to severe consequences such as bankruptcy and devaluation of a company's stock price [2]. Considering the failure consequences of centrifugal pumps, centrifugal pump fault diagnosis is of utmost concern. Faulty bearings, mechanical seal related faults, and impeller defects are the primary reasons for catastrophic failure of centrifugal pumps [2]. Numerous studies have been conducted to identify bearing defects [3]–[6]. However, very few research studies are available on the diagnosis of mechanical seal and impeller defects. Therefore, a diagnosis framework considering the defects of mechanical seals and impellers is

The associate editor coordinating the review of this manuscript and approving it for publication was Qichun Zhang.

required to enhance the reliability and safety of centrifugal pumps [7].

Generally, centrifugal pumps under an aberrant state are characterized by changes in their overall vibration level. Recently, vibration signals became very popular for developing diagnostic techniques for rotating machines, including centrifugal pumps [8]–[10]. The vibration signals have the intrinsic merit of revealing the failures in rotating machines [1]. Several research studies have been published that deal with the identification of fault characteristics in centrifugal pumps by analyzing the vibration signals. Sakthivel *et al.* [9] proposed a diagnosis technique for identifying the fault states of a mono-block centrifugal pump by combining statistical feature analysis with several Machine Learning (ML) approaches, i.e., k-Nearest Neighbor (k-NN), Decision Tree (DT), and Naïve Bayes. Unsworth *et al.* [11] utilized Fast Fourier Transformation (FFT) based analysis to identify centrifugal pump defects. Farokhzad *et al.* [12] suggested a DT-based intelligent approach to identify health features and used linear classification for final diagnosis. Muralidharan and Sugumaran [7] developed a DT based approach by utilizing the time-frequency domain method, Discrete Wavelet Transformation (DWT). However, with DT, such types of time-frequency analysis come at a high computational cost. Sun *et al.* [13] performed cyclic spectral analysis of the vibration signals for identifying centrifugal pump faults. Zheng and Xin [14] utilized geometry mode decomposition with power spectral entropy for fault feature extraction from hydraulic pumps. Yang *et al.* [15] proposed a framework based on refined composite multivariate multiscale symbolic dynamic entropy for centrifugal pump fault classification. Qiu *et al.* [16] proposed a Fisher discriminant ratio based fault feature selection technique in combination with a Support Vector Machine (SVM) to classify the health conditions of a centrifugal pump. Farokhzad *et al.* [17] developed a diagnostic technique for mechanical pumps by utilizing the FFT and a back propagation neural network. Wang and Chen [18] proposed a Wavelet Packet Transform based analysis with a Partially-Linear Neural Network (PLNN) for automatic health state classification of centrifugal pumps. Altobi *et al.* [19] utilized a hybrid of genetic algorithm, BP, and SVM for centrifugal pump fault diagnosis. For preprocessing of the signals, the one–dimensional (1-D) Continuous Wavelet Transform (CWT) method was considered. These diagnosis methods primarily extract statistical indicators or features from the time, frequency, or time-frequency domains of the vibration signals and use them to train classical ML algorithms for fault diagnosis purposes. These features may fail to recognize incipient faults and respond differently to different fault types. Therefore, feature extraction and feature selection largely affect the diagnosis performances of such methods. An improper choice of features can lower diagnostic accuracy and produce unreliable results. Moreover, a huge amount of domain expertise is required to implement the feature extraction techniques and not all of them can capture the nonlinear and non-stationary behavior of the centrifugal

pump vibration signals collected under various health conditions. Therefore, to overcome these shortcomings, deep learning-based approaches have been proposed.

Deep learning algorithms perform autonomous feature extraction from different domains and minimize the dependency upon extraction or selection of appropriate features. Deep learning is a recent research direction in fault diagnosis of rotating machines. Li *et al.* [20] developed a diagnosis method based on multisensory data fusion and a Convolutional Neural Network (CNN) for the health state classification of centrifugal pump faults. Zhao *et al.* [2] proposed an automated diagnosis system by using deep learning and soft max regression analysis. However, these studies used the sensor data directly which contain significant noise and lead to poor generalization of deep learning algorithms, especially for real world datasets. The research work [21] proposed a similar technique for sensor fault diagnosis, wherein, a computer software was used for the generation of faulty sensor data and after generating the faulty data, the signal recognition problem was transformed into an image recognition problem using CWT. The fault in the sensor was identified by using CNN with an accuracy of 99.6%. Despite the good accuracy, the nature of sensor faults is very different from that of the vibration response of centrifugal pump mechanical faults. Faults in the sensor affect the output of the sensor. Based on nature of the sensor output, these faults are categorized into drift fault, hard-over fault, erratic fault, spike fault, and stuck fault. Generally, the signal exhibits different behavior under different sensor fault conditions. In one case, the signal is composed of repeated individual spikes. In another case, the sensor faults cause an increase in variance of the successive signal samples. In yet another case, the sensor signals provide a constant value above the normal condition level, over a period. Depending upon the type of sensor fault, the signal either remains stationary or becomes non-stationary in nature [22].

On the contrary, in the case of centrifugal pumps, the mechanical faults produce shocks or impulses (of short duration) resulting in variation of the vibration signal amplitude and distribution. These mechanical faults induce a range of high to low frequencies into the signal which include system resonance frequencies, characteristic fault frequencies, rotor frequencies and their harmonics. These variations in the vibration signal change the stationary signal into a strictly non-stationary signal. Furthermore, the amplitude of these impulses is often overwhelmed by unnecessary macrostructural vibration of the centrifugal pump [23]. To overcome the non-stationary behavior of the vibration signal and unnecessary macro-structural vibration time-frequency domain techniques such as CWT can be used to extract discriminant features for CP fault diagnosis. Research available on centrifugal pump fault diagnosis using deep learning techniques is scarce and its full potential for the same is yet to be explored.

Mechanical faults in the centrifugal pump can be categorized into hard faults and soft faults. Hard faults are easy

to identify, however, soft faults are difficult to identify [24]. These soft faults in the centrifugal pump due to mechanical seal hole, mechanical seal scratch, and impeller defect will lead not only to performance degradation but also to potential safety hazards [25]. Majority of the existing studies [3] oriented themselves to diagnosis of bearing defects and limited attention was given to soft faults diagnosis. For mechanical soft faults, the fault frequencies are often vanished by the noise due to their soft nature. For this reason, an automated fault diagnosis [26] is needed which primarily focuses on the early identification of soft faults due to mechanical seal hole, mechanical seal scratch, and impeller defects. To address the above-mentioned problem, in this paper, a new hybrid approach based on signal to time-frequency image conversion and deep learning is introduced to identify the health states of centrifugal pumps under soft fault conditions. Deep learning algorithms are quite effective in detecting image features automatically [27]. First, the time domain vibration signals acquired from the centrifugal pumps are processed with continuous wavelet transform to form scalograms (CWTS). The scalograms capture the fault information contained in vibration signals over different time and frequency scales. The CWTS are further converted into gray-scale images to provide computational benefits to the deep learning classifiers. Afterwards, an improved version of convolution neural network called as Adaptive CNN (ADCNN) is proposed to process the scalograms and identify the pump conditions. The main contribution of this research paper is highlighted as follows:

1. The potential of continuous wavelet transform scalogram (CWTS) images in centrifugal pump fault diagnosis is validated through experimental signals acquired from a real-world centrifugal pump test bed. A new signal to time-frequency imaging technique is proposed that extracts CWTS images from 1D vibration signals and converts them into 2D grayscale images (CWTSGI) for further analysis. To the best of the author's knowledge, CWTS images have rarely been applied to centrifugal pump fault diagnosis.

2. ADCNN architecture is utilized to automate the feature extraction and classification processes. The use of an ADCNN eliminates the need to extract separate features and choose the best ones from among them. An adaptive learning rate is considered in the training phase of the ADCNN for avoiding convergence to a local minimum, which in turn is essential for maximizing its diagnostic performance.

3. Soft faults in centrifugal pumps such as mechanical seal defects and impeller defects have been considered for analysis.

The rest of this paper is organized as follows: Section 2 provides the background information for the CWTS and the CNN network. The details of the proposed centrifugal pump test bed and diagnosis procedure are provided in Section 3. Section 4 discusses the experimental results. Finally, the research paper is concluded in Section 5.

II. TECHNICAL BACKGROUND
This section describes the theoretical background of the CWTS and the CNN.

A. CONTINUOUS WAVELET TRANSFORM SCALOGRAM
Time-domain and frequency-domain analysis are commonly exploited to diagnose the faults in rotating machines such as centrifugal pumps. However, both fail to depict the signal variations in time and frequency scales simultaneously. In practical cases, the signals acquired from centrifugal pumps are non-stationary and non-linear in nature [4], [28]. Therefore, time-frequency analysis serves as an effective approach to extract the fault information hidden in the centrifugal pump signals in the form of images [29]. The time-frequency domain method decomposes the signals over different time and frequency scales, which are then represented as a two-dimensional image. The image contains the local (specific regions of the image) and global (entire image) characteristics of the signal. Furthermore, such two-dimensional images act as competent input features for deep learning algorithms and improve their diagnostic accuracy. Hence, it is of great significance to consider the time-frequency approach for analyzing the centrifugal pump vibration signals.

In this paper, the CWT has been adopted to process the pump signals. CWT utilizes a family of mother wavelet functions to transform the input signal into a spectrum of wavelet coefficients. This is achieved by translating and scaling the original signal over different time and frequency levels. The occurrence of faults produces multiple low to high frequencies in the original signal and hence, the energy content varies over different frequency ranges. Through CWT, the energy of the original signal gets distributed over the decomposed signals which in turn helps to identify the time-frequency scales with substantial energy content. As such, the wavelet coefficients can be used to provide an insight into the health conditions of mechanical components [30], [31]. The details of CWT can be expressed by the following mathematical expressions:

$$\gamma_{p,q}(t) = |p|^{-\frac{1}{2}} \gamma \left(\frac{t-q}{p} \right) \quad \text{where } p, q \in R, \text{ and } p \neq 0$$

$$(1)$$

$$T(p,q) = C_p(k) = \int x(t) \overline{\gamma}_{p,q}(t) \, dt \qquad (2)$$

where $\gamma_{p,q}(t)$ is the mother wavelet function, the shape and displacement of the wavelet function are ascertained by the scale parameter p and the translation or location parameter q, $x(t)$ is the original signal, the wavelet coefficients at the pth scale is C_p where $p = 1, 2, 3, \ldots, l$, $\overline{\gamma}_{p,q}(t)$ is the complex conjugate of $\gamma_{p,q}(t)$ at scale p and location q, and finally $T(p,q)$ denotes the CWT of the signal. When the wavelet correlates well with signal $x(t)$ at a given p and q, then a large magnitude of $T(p,q)$ is obtained [26]. In the CWT approach, among all the wavelet families, the Morlet wavelet is preferred [32]. To represent these wavelet coefficients at

different (p,q) scales, the scalogram of the CWT is proposed [31]. A scalogram depicts the CWT coefficient of a signal in two-dimensional time-frequency plot. The x-axis of a scalogram denotes the translation or time parameter whereas the y-axis reflects the scale parameter that holds a reciprocal relationship with the frequency of signal. The color intensity of a pixel in the scalogram plot is proportional to the absolute value of the wavelet coefficient. Thus, the scalogram implies how energy in the original signal is distributed in the time-frequency plane [33]. Thus, CWT assists in capturing the localized energy variations over different regions of the two-dimensional time-frequency image. Therefore, intuitively, CWT scalograms (CWTS) can discriminate different health conditions of the centrifugal pump by interpreting the wavelet coefficients as time-frequency image features.

B. CONVOLUTIONAL NEURAL NETWORK (CNN)

The CNN architecture is usually formed with one input layer, a few convolution layers and pooling layers, several fully connected layers, and one final output layer to automate the feature extraction process [34]. The CNN successfully captures the spatial and temporal dependencies of an image through its different layers and preserves the features important for classification in a computationally powerful manner [35]. Additionally, incorporation of several optimization techniques in the recent few years that include Batch Normalization (BN), Dropout (DL), and Rectified Linear Units (ReLU) has improved the performance of CNNs [36]–[39]. The training process for a CNN is implemented in two stages, forward propagation stage and backward propagation stage. In the forward propagation stage, the CNN architecture extracts the spatial information from the input image throughout the designed layers [29]. In the backward propagation step, the network tries to update the internal parameters in order to optimize the given objective function [40]. From the previous literature available on CNN, it is obvious that there is no rule of thumb for selecting the best number of layers in a CNN and the selection process for the total number of layers is a train-test based approach and is dependent on the nature of the input data. The forward and backward propagation are further explained as follows:

1) FORWARD PROPAGATION
a: CONVOLUTION LAYER

In this step, the Convolution Layers (CLs) learn the abstract features from the input image data to retain the relationship between pixels of the input while learning image attributes [29]. To achieve an enhancement of these convoluted features, an activation function with added weights and biases is applied [40]. This whole process can be expressed by the following relation:

$$x_n^m = f\left(\sum_{i\in K_n} x_i^{m-1} * w_{in}^m + b_n^m\right) \tag{3}$$

where x_n^m is the mth component of layer n, K_n is the nth convolution region of the $m-1$ layer feature map, w_{in}^m is the weight

matrix, and b_n^m is the added bias. After calculating the summation of the total operation as described into Eq. (3), a nonlinear activation function f, called Leaky RELU, is applied on it. This function can be written as:

$$f(x) = \max(0.1x, x) \tag{4}$$

b: POOLING LAYER

Immediately after the CLs, a Pooling Layer (PLs) is added to decrease the redundancy of the extracted features from the previous layer. In this study, max pooling is used as the pooling layer [41], which can achieve the maximum value of the convolutional output x_n^m as follows:

$$x_n^m = f\left(w_n^m * \max(x_n^{m-1}) + b_n^m\right) \tag{5}$$

where, the output x_n^m of the convolution layer is down sampled, w_n^m, and b_n^m represents the weight and bias matrix, respectively. The $\max(x_n^{m-1})$ denotes the max pooling function used to lessen the dimensions of the attained convoluted feature maps.

c: FULLY CONNECTED LAYER

To increase the depth of the network architecture, several CLs and PLs are stacked together. Usually, several Fully Connected Layers (FCLs) are arranged layer by layer till the final one is reached, which alters the resultant filter matrix to a column or row [42]. Thus, at the end, the output feature can be obtained by the final fully connected layer which is given as:

$$y^z = f\left(w^z x^{z-1} + b^z\right) \tag{6}$$

where z represents the continuous order of the network architecture and y^z is the output of the final fully connected layer, f is the activation function to give the probabilistic output from the input. In this research paper, SoftMax [42] is considered as the final activation function.

2) BACKWARD PROPAGATION

After completion of the forward propagation, the objective function (commonly known as, loss function) is calculated to acquire the target data in accordance with the input data. Once the loss function is calculated, the parameters (i.e., weights, and biases) of the network architectures are updated in a reverse manner. This is achieved by propagating the loss function error in the backward direction. In this study, the cross-entropy loss function [40] can be expressed as follows:

$$E(w) = \frac{1}{n}\sum_{z=1}^{n}\left[y_z \ln \overline{y_z} + (1-y_z)\ln(1-\overline{y_z})\right] \tag{7}$$

where y_z and $\overline{y_z}$ are the actual target and the predicted value of the zth sample, respectively.

During the training process, the stochastic gradient descent method is utilized to minimize the loss function and update the network weights and biases. While training the neural network, the entire input dataset is divided into several smaller

groups called batches, and multiple batches are supplied to train the CNN [43]. Thus, to minimize the loss function and avoid overfitting or underfitting problems, the entire training process is realized over several epochs [39], [43].

III. PROPOSED METHODOLOGY

As discussed before, it has been proposed to utilize CWTS and ADCNN to diagnose the health states of pumps. Figure 1 shows the workflow diagram of the proposed approach. The proposed approach consists of three main steps, (1) Data collection, (2) Data Preprocessing, and (3) Diagnosis. These steps have been described in detail in the following sections:

A. DATA COLLECTION TROUGH A TESTBED DESIGNED FOR A CENTRIFUGAL PUMP

A test setup is developed to collect the vibration signals from different pump health conditions for diagnosis purposes. Figure 2 shows the schematic details of the test setup. The test setup consists of a main tank and a buffer tank interconnected with each other. The main tank supplies water to the buffer tank. A mechanical pump of model PMT-4008 [44] is linked to the buffer tank through a valve and a strainer. The valve is attached to the buffer tank for adjusting the intake flow rate. The pump speed (RPM), intake flowrate, temperature, and pressure conditions are controlled throughout the entire experiment. The vibration data is measured with two accelerometer sensors mounted at suitable locations on the centrifugal pump, as shown in Figure 2(a) and 2(b). A Data Acquisition System (DAQ) developed by National Instruments (model NI 9234) [45] is connected to the vibration sensors through cables and is utilized to record the vibration signals. Data is acquired with a sampling frequency

of 25.6 kHz at a constant speed of 1733 RPM. The vibration dataset is gathered under two different pressure conditions (3.0 bar, and 4.0 bar). For each pressure condition, four types of health states were considered, namely, healthy (normal), impeller crack, mechanical seal hole, and mechanical seal scratch. For each health condition, 1,000 signals were recorded. The faults were introduced artificially into the corresponding components of the centrifugal pump. Figure 3 presents an original view of the artificially seeded defects. Further, the detailed description of the collected vibration datasets is provided in Table 1. As can be seen from Table 1, two complete datasets under different pressure conditions and four health conditions, denoted as Normal Condition (NC), Impeller Crack (IC), Mechanical Seal Hole (MSH), and Mechanical Seal Scratch (MSS) have been utilized for validating the performance of the proposed diagnostic framework.

B. DATA PROCESSING BY CWT-SCALOGRAM BASED GRAY SCALE IMAGING (SGI)

Preprocessing of vibration signal plays a vital role, particularly in neural network-based fault diagnosis techniques [46]–[48]. In this step, the CWT Scalogram-based Gray Scale Imaging (CWTSGI) approach is applied for preprocessing of the collected vibration signals. The CWTSGI framework is executed into two steps, (i) The acquired time-domain vibration signals are decomposed via the CWT and two-dimensional CWTS images are obtained. The CWTS retains the information about the energy distribution across the time-frequency plane for different health conditions [32], [49], [50], and (ii) the resulting CWTS images are converted into gray-scale images using a weighted sum of the red, green, and blue intensity pixels [51]. This adds
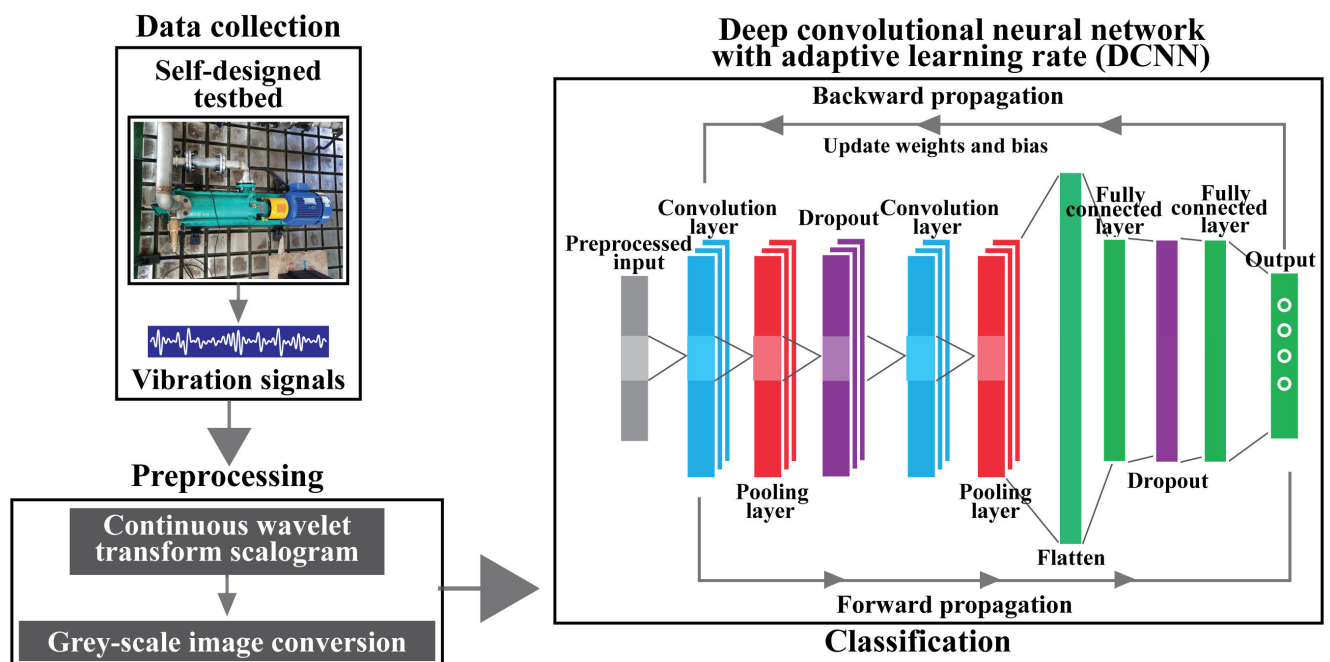

FIGURE 1. The workflow diagram of the proposed fault diagnosis method.
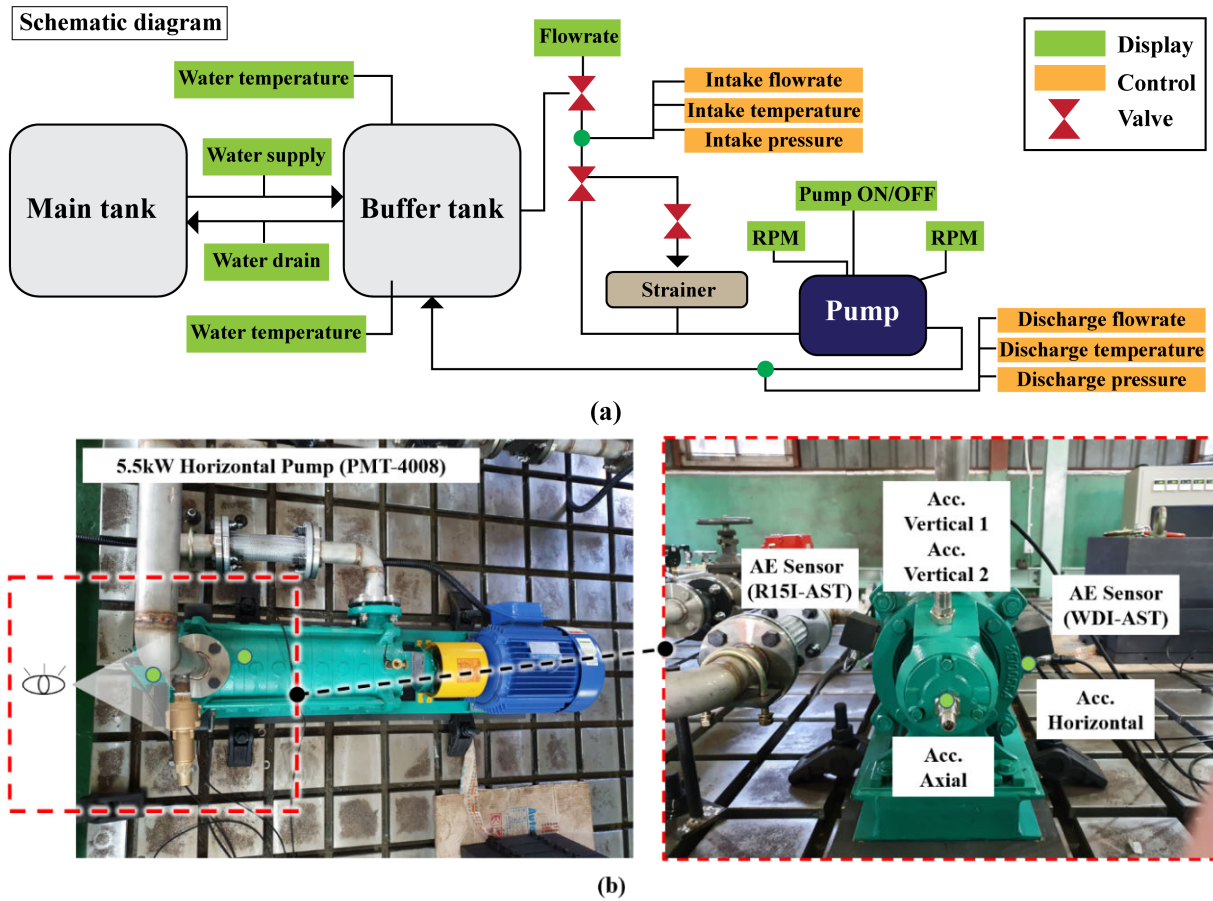
FIGURE 2. (a) The schematic diagram of the experimental testbed, (b) specifics of the sensor location of the pump.

TABLE 1. Specifics of the datasets.

	Health Type	Crack Size (mm)			Pressure (Bar)	Samples
		Diameter (mm)	Length (mm)	Depth (mm)		
Dataset 1	Normal Condition (NC)	-	-	-	3.0	1000
	Impeller Crack (IC)	2.5	18	2.8		1000
	Mechanical Seal Hole (MSH)	2.8	-	2.8		1000
	Mechanical Seal Scratch (MSS)	2.5	10	2.8		1000
Dataset 2	Normal Condition (NC)	-	-	-	4.0	1000
	Impeller Crack (IC)	2.5	18	2.8		1000
	Mechanical Seal Hole (MSH)	2.8	-	2.8		1000
	Mechanical Seal Scratch (MSS)	2.5	10	2.8		1000

computational benefits for the neural network-based analysis. For simplicity, these images have been referred to as SGI in the paper. In order to meet the size restraints of the developed ADCNN architecture, the SGI's are constricted [29]. Therefore, each SGI is compressed into $256 \times 256 \times 1$ dimensions. The SGI helps to visualize the different health states of the mechanical pump possessing distinct CWTS patterns.

C. DIAGNOSIS THROUGH ADAPTIVE DEEP CONVOLUTIONAL NEURAL NETWORK ARCHITECTURE (ADCNN)

In this step, the SGI's are provided as an input to the proposed ADCNN for centrifugal pump health state identification and classification. The ADCNN consists of a CNN structure illustrated in Figure 4.
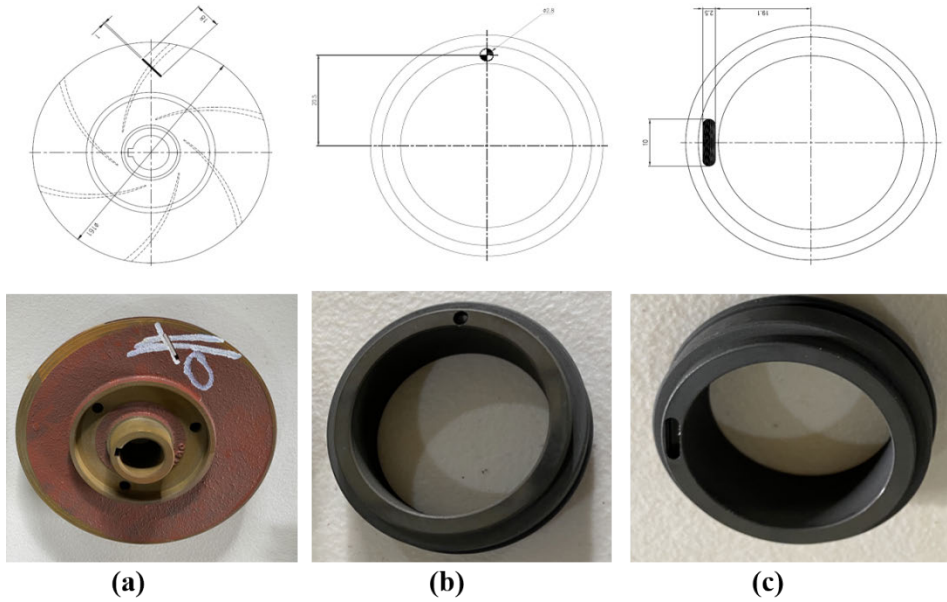
FIGURE 3. Specifications of different faults, i.e., (a) impeller crack, (b) mechanical seal hole, and (c) mechanical seal scratch.
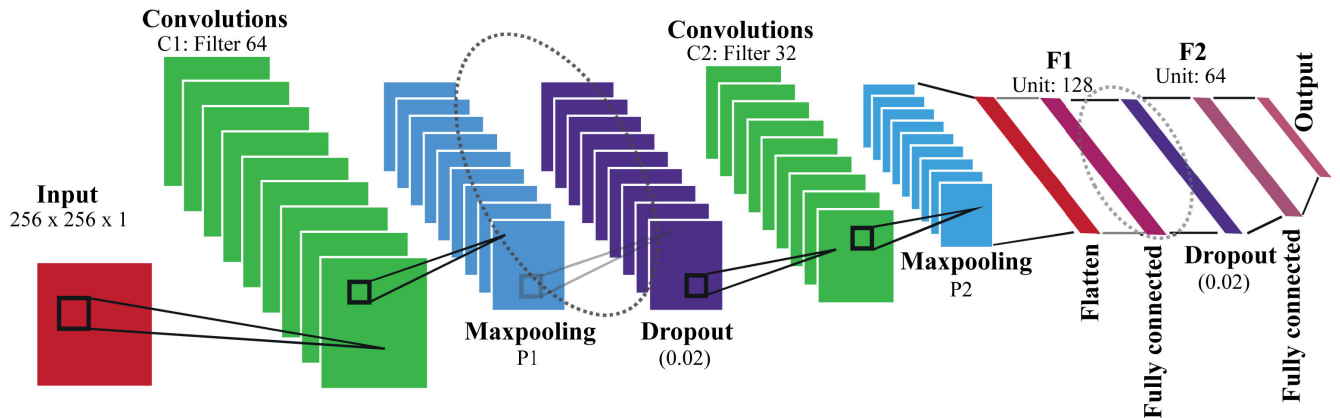

FIGURE 4. Architecture of the proposed neural network (ADCNN).

The proposed ADCNN architecture can be explained as follows: the ADCNN has a total of ten layers which starts with the input layer followed by a total of two CLs. After CLs, the architecture has two PLs, two DLs, two FCLs and finally one output layer. The size of the input layer is determined according to SGI's ($256 \times 256 \times 1$). To reduce the number of parameters and to enhance the training efficiency the kernel size is determined to be 5×5. The CL1 and CL2 consist of 64 and 32 filters. The CL1 size is down sampled by the PL2. The FCL1 merges all the feature maps of the CL2 into a 1-D form. The FCL2 facilitates the final layer to classify the input data into its respective classes. The valid convolution method utilized in this neural architecture accepts the size of the feature maps to remain unchanged. Furthermore, the two dropout layers allow the network to generalize data to reduce over-fitting problems [36], [38]. As mentioned earlier, the training process of the neural network is conducted through the Backward Propagation Stage (BPS). The main goal of training the network is to minimize the objective

function error by updating the weights and biases through the BPS. In the training stage, a deep learning rate is considered to provide the DCNN structure. This deep learning can optimize the performance of the neural network and avoids the convergence of the objective function to a local minimum. Furthermore, for updating the weights into the DCNN, an adaptive moment estimation method (Adam) is considered [52]. Adam combines the advantages of deep gradient algorithms (AdaGrad) to deal with the sparse gradients and a root-mean-square propagation (RMSProp) algorithm capable of performing at non-stationary settings. Adam preserves the exponential moving averages (EMA) of the gradient and its square in every update, which are related as follows:

$$w = w - \alpha \frac{B_{mt_1}}{\sqrt{B_{mt_2} + \varepsilon}} \tag{8}$$

where,

$$B_{mt_1} = \beta_1 B_{mt_1-1} + (1 - \beta_1) \frac{\partial}{\partial w} \cos t(w) \quad \text{here } \beta_1 \approx 1 \tag{9}$$

$$B_{mt_2} = \beta_1 B_{mt_2-1} + (1 - \beta_2) \frac{\partial^2}{\partial w^2} \cos t\,(w) \quad \text{here } \beta_2 \approx 1 \tag{10}$$

where w is the weight parameter and α is the positive scalar step size. Here, B_{mt_1} and B_{mt_2} are the first and second moment bias correction respectively and β_1, β_2 are the decay rates. From Eqs. (9) - (10), it is observable that the step size α and decay rates β_1, β_2 are small. Thus, the weight update process described into Eq. (8) offers a nearly optimal learning rate selection [52]. Therefore, the final structure combining the CNN, the deep learning rate, and Adam is referred to as ADCNN in this paper. Finally, to tune the hyperparameters (i.e., dropout rate, learning rate, momentum, number of epochs, and number of batch size) of the proposed architectures a grid search based 5-fold Cross Validation (5-CV) is used. The details of the proposed ADCNN with layer specifications are given into Table 2.

D. FOR THE DIAGNOSTIC PERFORMANCE ASSESSMENT

The performance of the proposed fault diagnosis framework can be validated by considering several performance criteria,

which are as follows: (1) precision (P) [53], (2) recall (R) [54], (3) F1 score (F1) [53], (4) final accuracy (FA), (5) confusion matrices [55], (6) graphs of the objective (loss) function, and (7) feature space obtained by t-stochastic Neighbor Embedding (t-SNE) for the output layer of the CNN, which demonstrates class separability [56]. P, R, F1, and FA can be obtained by the following equations:

$$P = \frac{TP}{TP + FP} \tag{11}$$

$$R = \frac{TP}{TP + FN} \tag{12}$$

$$F = \frac{2TP}{2TP + FN + FP} \tag{13}$$

$$FA = \frac{TP + TN}{TP + TN + FN + FP} \tag{14}$$

In Eqs. (11) - (14), the terms TP, TN, FN, and FP represents true positive, true negative, false negative, and false positive, respectively. While measuring the diagnostic output of the proposed ADCNN, the confusion matrix demonstrates the real overview of the actual vs. predicted output and shows the clarity of the performances.

TABLE 2. The proposed ADCNN structure Table 1.

Layers	Parameters	Observations	Height	Width	Depth	Parameters Trainable
Input		Preprocessed Signals	256	256	1	
Convolution 1	Kernel Size	Filter	3	3		Yes
	Padding	Zero				
	Depth	Filter number			64	
	Output		256	256	64	
Pool 1	Kernel Size	Filter	3	3		No
	Padding	Zero				
	Output		85	85	64	
Dropout	Output		85	85	64	No
Convolution 2	Kernel Size	Filter	3	3		Yes
	Padding	Zero				
	Depth	Filter number			32	
	Output		85	85	32	
Pool 2	Kernel Size	Filter	3	3		No
	Padding	Zero				
	Output		28	28	32	
Dropout	Output		28	28	32	No
F1	Nodes	Flatten into 1D	128			Yes
F2	Nodes	Flatten into 1D	64			Yes
Output	Nodes	Flatten into 1D	4			Classify

IV. EXPERIMENTAL VERIFICATION—RESULTS AND DISCUSSIONS

The proposed diagnostic framework (CWTSGI + ADCNN) is applied on the vibration data collected from the centrifugal pump testbed. In this study, the vibration signals are collected from the self-designed experimental testbed for two different pressure conditions (pressure 3.0 bar and pressure 4.0 bar). For each pressure condition, a total of 4,000 samples were collected from each health types with a sampling rate of 25.6khz. Out of these 4,000 samples, 1,000 samples of 1 second were collected under normal operating condition, denoted as NC. Similarly, from each of the other health conditions (i.e., Impeller Crack (IC), Mechanical Seal Hole (MSH), and Mechanical Seal Scratch (MSS)), 1,000 samples of 1 second are collected. Thus, a balance dataset has been formed for final analysis. The details of this dataset configuration have already been described into Table 1. Moreover, Figure 5 depicts the original time-domain signals for different health conditions under two different pressure conditions. From this time-domain signal, it is very difficult to visualize the differences between the time-domain vibration signals for different health conditions. Further, the time-domain vibration signals may contain noise or random fluctuations that can mask the fault information contained in the vibration signals.

To retain the fault features visually, the CWTS is applied to the vibration signals. Figure 6 portrays the CWTS of vibration signals acquired under different health conditions at pressures of 3.0 bar and 4.0 bar, respectively. From this Figure 6, no significant meaning can be captured related to the change of amplitude of the signal along with the time. Therefore, Figure 7 presents the contour plots of the corresponding CWTS images to provide a better visualization of the alterations in CWTS patterns for different health conditions. It can be realized from Figure 6 and 7 that the CWTS images

have distinctive patterns across various time-frequency scales for each of the health conditions. For dataset 1 (pressure 3.0 bar), it can be observed that the CWT coefficients possess large magnitudes at lower frequency scales and the energy of vibration signal is mainly concentrated around the lower frequency regions, when the vibration signal is in healthy condition. For the MSH and MSS types fault, the in-plane torsional vibrations and out-plane lateral vibrations produce additional frequency modes into the vibration signals [57]. Thus, the energy of the vibration signal spreads across the different frequency scales in the CWTS plots, ranging from low to high.

The IC fault increases the vibration signal amplitude at higher harmonics of the pump rotational speed. Hence, the energy content is found to be larger in some of the higher frequency scales. Hence, the CWTS patterns for NC, MSH, MSS, and IC are clearly distinguishable from each other for pump vibration dataset 1 acquired under a pressure of 3 bar. In the case of dataset 2 (pressure 4.0 bar), the energy fluctuations across the different frequency modes are relatively smaller under different health conditions as compared to that of dataset 1. However, the CWTS manages to capture the minor variations along the frequency scales, which is almost impossible with the use of traditional feature extraction methods. In addition, the variation along the timescales is clearly separable between the CWTS plots for different fault types. The energy is more concentrated across the timescales for faulty conditions as compared to the healthy state. The CWTS images are converted to SGI format (CWTSGI) and supplied to the ADCNN network for diagnosis of pump faults.

Finally, two experiments were conducted for datasets 1 and 2 mentioned into Table 1 for evaluating the diagnostic performance of the proposed approach. For experiment 1, 60% of dataset 1 from each health class is used for learning the
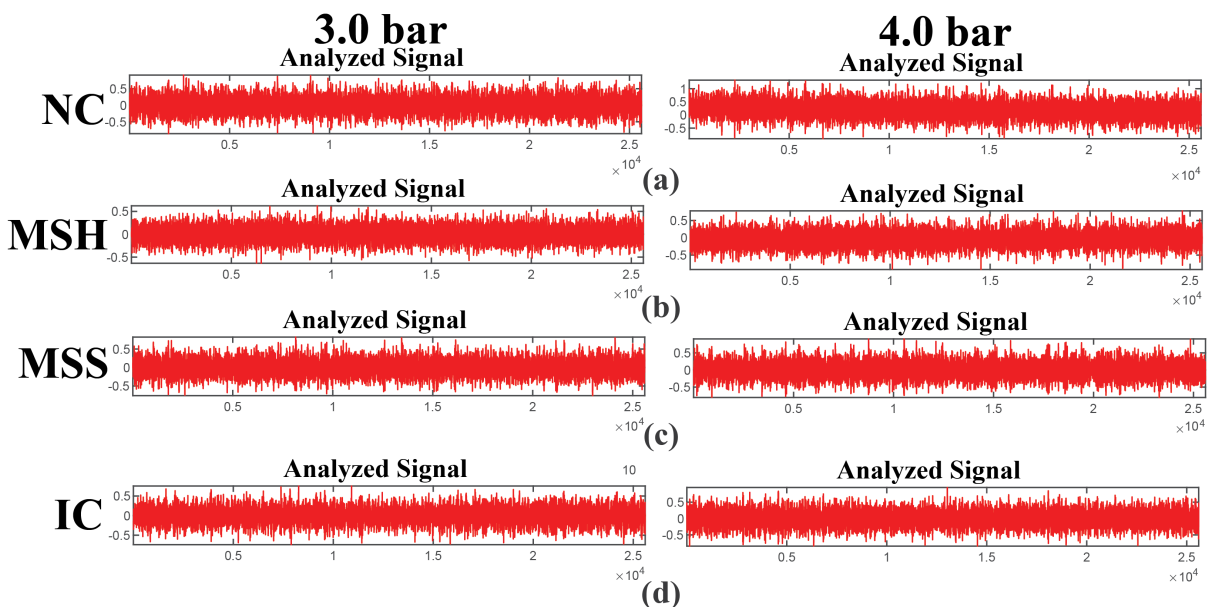

FIGURE 5. Time domain vibration signals of different health types, i.e., (a) normal condition (NC), (b) mechanical seal hole (MSH), (c) mechanical seal scratch (MSS), and (d) impeller crack (IC).
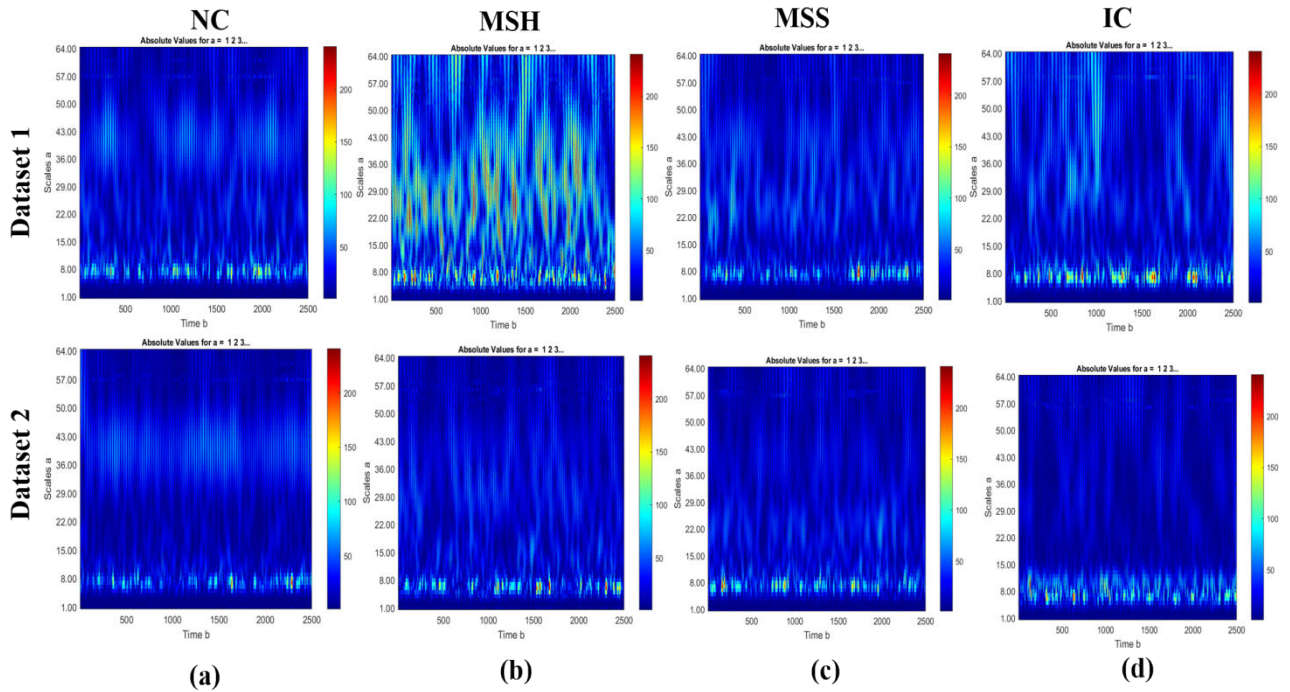
FIGURE 6. The CWTS for vibration signals of different health states, (a) normal condition (NC), (b) mechanical seal hole (MSH), (c) mechanical seal scratch (MSS), and (d) impeller crack (IC).
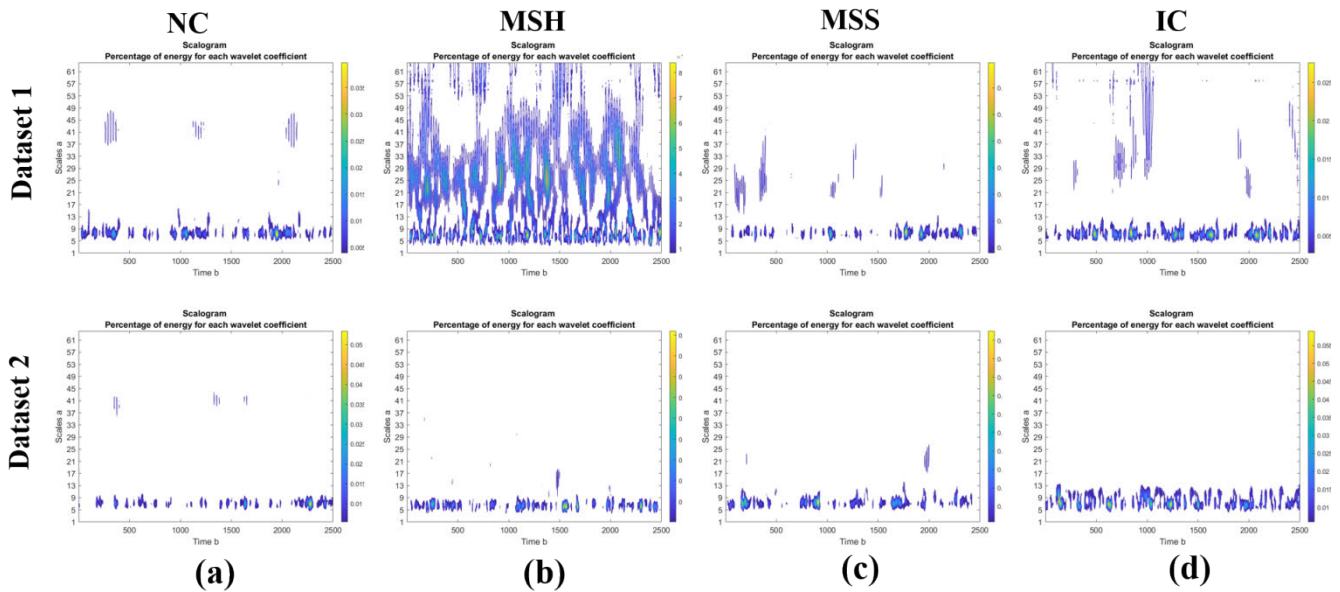

FIGURE 7. Contour plots of the CWTS of different health types, i.e., (a) normal condition (NC), (b) mechanical seal hole (MSH), (c) mechanical seal scratch (MSS), and (d) impeller crack (IC).

CWTS patterns and the other 40% is used for testing the network. The network again divides 60% of the learning data into 80% for training and 20% for validation. For experiment 2, dataset 2 is utilized, which is again divided in a similar manner as dataset 1. The details of the training, testing, and validation datasets are provided in Table 3.

For each set of the experiments, an appropriate learning rate is an essential constraint for optimization of the training process to achieve better generalization and performance. Figure 8 compares the convergence rates of a

DCNN architecture and a 5-layered straight forward basic CNN model [27] assuming a fixed learning rate of 0.05 for both of them. It can be observed that the DCNN nearly converges to zero while the traditional CNN does not. Such a behavior is expected in a network with better classification accuracy. However, in this paper, the learning rate has been allowed to adapt itself during the training process for further improvement. Therefore, by considering the ADCNN architecture for final diagnosis purpose, the performance of the proposed approach is validated with experiments 1 and 2.
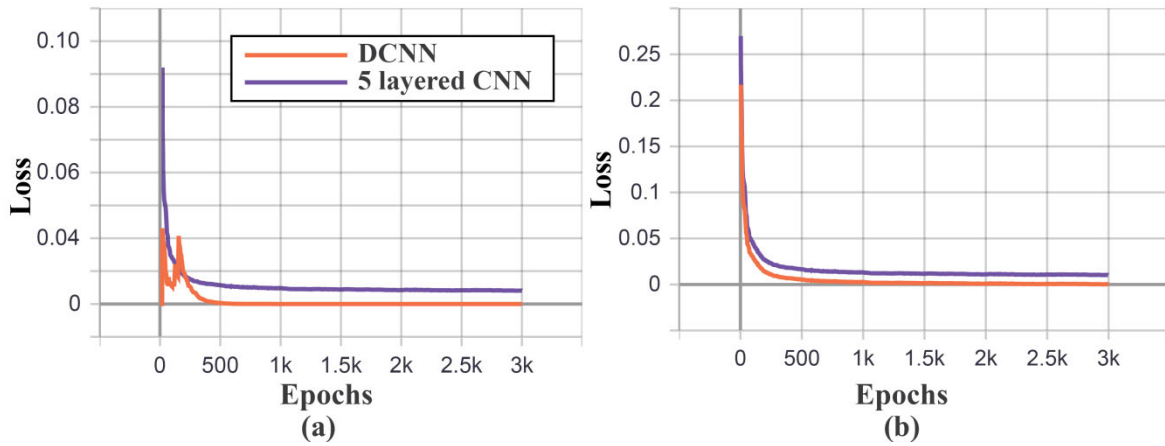
FIGURE 8. Cost function (loss) convergence rate of the DCNN, and 5 layered CNN for the training data at a learning rate of 0.05 for (a) experiment 1 – dataset 1, and (b) experiment 2 – dataset.
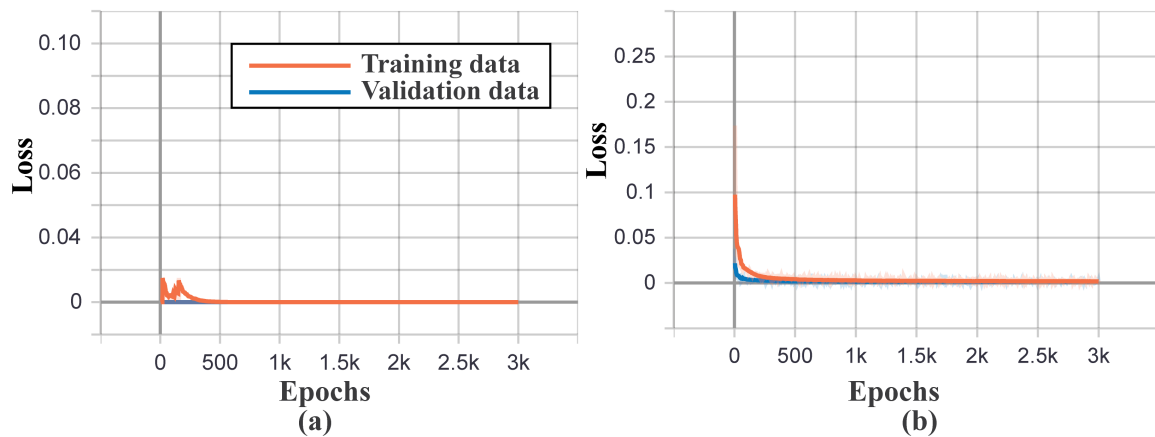

FIGURE 9. Behavior of the loss functions while training the ADCNN for two experiments, (a) experiment 1 – dataset 1, and (b) experiment 2 – dataset 2.

TABLE 3. Data division.

Dataset	Training (60%)		Testing
	Training (80%)	Validation (20%)	(40%)
1	1920	480	1600
2	1920	480	1600

For this purpose, the parameters discussed into Section 3.4 are utilized. Moreover, to select the best Dropout rate, learning rate and momentum, grid search approach is considered. Table 4 provides the details of the diagnostic performance. It can be realized from Table 4 that the proposed approach achieved 100% classification accuracies in the corresponding health states or classes for both the experiments. Therefore, it is proved that the proposed approach based on CWTSGI and ADCNN can distinguish among different health classes for centrifugal. While training the network, the behavior of the loss function is observed for 3000 epochs to ensure the bias-variance trade-off between the training and validation data. Figure 9 shows the behavior of the loss functions for

both sets of experiments. The validation curves tend to zero which indicates that the proposed DCNN tackled the overfitting and underfitting of the training data. Furthermore, at the end of the training, the class separability is verified by applying the t-SNE algorithm at the output layer. The t-SNE based feature space is depicted in Figure 10. Additionally, to revalidate the test performances, the confusion matrices are computed as shown into Figure 12. From all these performance analyses, it can be concluded that the proposed approach performed effectively on the centrifugal pump vibration datasets and can be utilized for better diagnosis of centrifugal pump faults.

The proposed approach is composed of time-frequency based imaging technique called CWTS and an automatic adaptive classifier, proposed as ADCNN. Therefore, to establish the robustness of the proposed approach, two points need to be validated, i.e., (i) the choice of time-frequency based technique over time-domain analysis and frequency-domain analysis, and (ii) the selection of automatic neural network-based classifier over traditional feature analysis based diagnostic methods. Therefore, the following methods are considered in this study for comparisons:

TABLE 4. Details of the diagnostic performance.

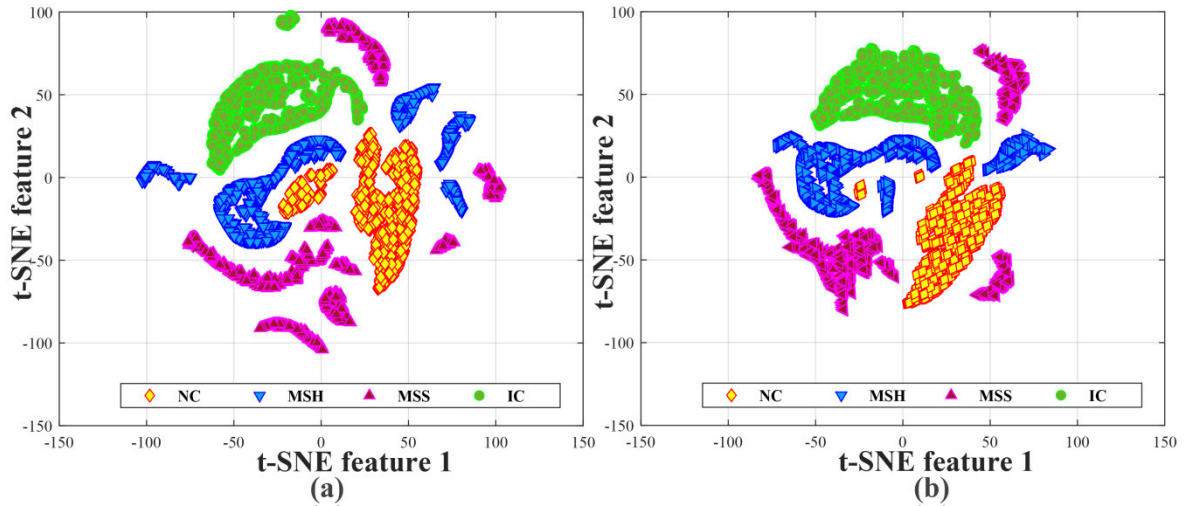| Exp.	Dataset	P (%)				R (%)				F (%)				FA (%)
		NC	MSH	MSS	IC	NC	MSH	MSS	IC	NC	MSH	MSS	IC	
1	1	100	100	100	100	100	100	100	100	100	100	100	100	100
2	2	100	100	100	100	100	100	100	100	100	100	100	100	100

FIGURE 10. Observation of the t-SNE feature space of the output layer while training, (a) experiment 1 – dataset 1, and (b) experiment 2 – dataset.
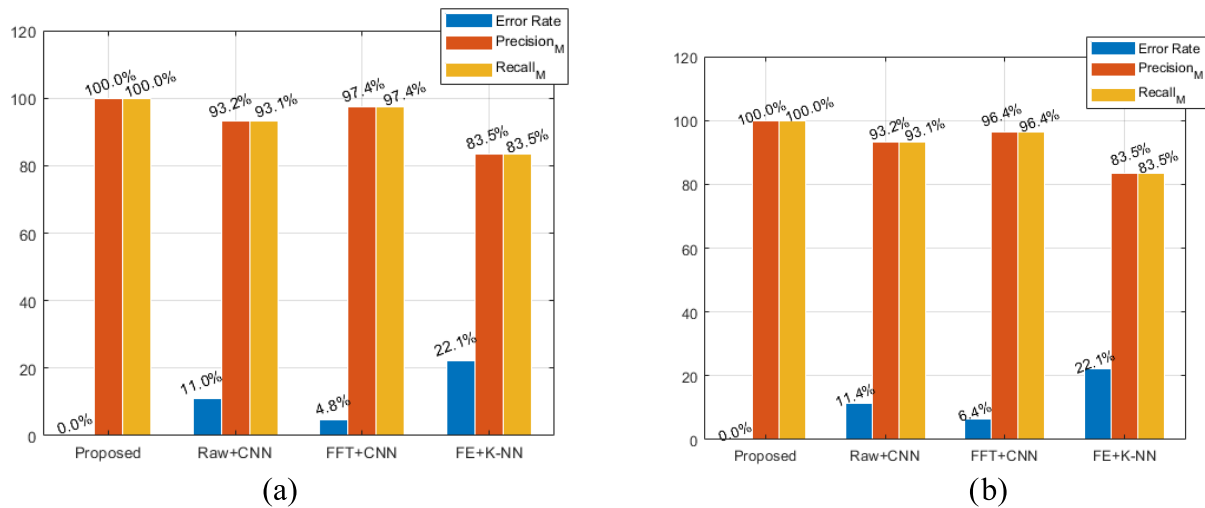

FIGURE 11. Evaluation of the proposed method against the reference methods, (a) experiment 1 – dataset 1, and (b) experiment 2 – dataset 2.

1) RAW + CNN: In this approach, the original raw 1D pump vibration signals are directly fed to the CNN network for fault diagnosis. This comparison validates the choice of time-frequency based analysis over the time-domain based analysis.

2) FFT (fast Fourier transform) + CNN: In this approach, the FFTs of the pump vibration signals are supplied to the CNN for fault diagnosis [58]. This comparison validates the choice of time-frequency based analysis over the frequency-domain based analysis.

3) FE + k-NN (Feature extraction + k-nearest neighbor): In this approach, the traditional statistical features from the time and frequency domains are used as inputs to k-NN for fault classification [5]. This comparison establishes the necessity of developing an automatic neural network-based classifier ADCNN over the traditional feature analysis based diagnostic methods.

Table 5 shows the comparison results along with the percentage improvement of the proposed method over the above-mentioned methods. The experimental dataset was

TABLE 5. Diagnostic performance comparison.

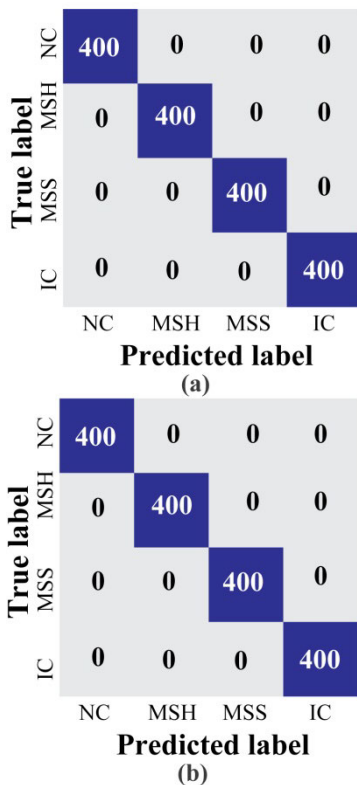| Method	Exp.	F (%)				FA (%)	Improvement
		NC	MSH	MSS	IC		(Proposed - Current)
RAW + CNN	1	94.1	94.6	93.8	93.2	93.9	6.1
	2	94.3	93.2	93.1	93.3	93.5	6.5
FFT + CNN [58]	1	95.2	95.3	95.1	94.3	94.9	5.1
	2	95.1	95.4	95.7	95.0	95.3	4.7
FE + k-NN [5]	1	85.3	84.2	84.9	83.1	84.4	15.6
	2	84.1	84.7	85.2	84.2	84.6	15.4

FIGURE 12. Observation of the confusion matrices for the test datasets, (a) experiment 1 – dataset 1, and (b) experiment 2–dataset 2.

kept identical for each of these comparison tests. The RAW + CNN approach achieved 93.9%, and 93.5% FA, for the experiment 1 and 2, respectively. Meanwhile, the frequency domain based FFT + CNN [58] approach performed better than the time-domain based analysis. For experiment 1, and 2, it achieved 94.9%, and 95.3% FA, respectively. However, the classical feature-based approach FE + k-NN performed very poorly for the considered dataset. It achieved 84.4%, and 84.6% FA, for experiment 1, and 2, respectively. Figure 11 shows the average error rate, micro precision, and micro recall of the proposed method against the reference methods. All these evaluation matrices were calculated using the formulas from [59]. The average error

rate, micro recall, and micro recall for classification of the proposed method is 0%, 100%, and 100% consecutively for dataset-1 as compared to RAW + CNN which is 11%, 93.2%, and 93.1%, FFT + CNN which is 4.8%,97.4%, and 97.4%, and FE + K-NN which is 22.1%, 83.5%, 83.5%. similarly, for dataset-2 The average error rate, micro recall, and micro recall for classification of the proposed method is 0%, 100%, and 100% consecutively as compared to RAW + CNN which is 11.39%, 93.26%, and 93.12%, FFT + CNN which is 6.43%,96.44%, and 96.4%, and FE + K-NN which is 22.08%, 83.50%, 83.50%. All These results indicate that the developed framework clearly outperformed the three state-of-art methods, yielding average improvements of 5.1 – 15.6% and 4.7 – 15.4% for experiments 1 and 2, respectively. The comparison results for the RAW + CNN and FFT + CNN [58] confirm the necessity of the vibration data preprocessing using the proposed CWTS-SGI technique. On the other hand, the comparison results for FE + k-NN [5] highlights the necessity of deep learning-based approaches such as ADCNN used in the present case.

V. CONCLUSION
This paper introduced a continuous wavelet transform (CWT) scalogram based imaging technique combined with an adaptive deep convolutional neural network (ADCNN) architecture for monitoring the health conditions of mechanical pumps. By incorporating the CWT scalogram based gray-imaging (SGI) with the proposed ADCNN architecture, the proposed approach makes full use of the abilities of the CWT to process the non-stationary, non-linear vibration signals and enables an end-to-end diagnosis framework without handcrafted feature analysis. Data collected from a self-designed centrifugal pump testbed are used to validate the performance of the proposed diagnostic framework. Experimental results suggest that the proposed framework can meaningfully enhance the diagnostic performance for pump faults. Furthermore, the proposed approach (SGI + ADCNN) provided better performance than the three state-of-art methods discussed above, namely RAW + CNN, FFT + CNN and FE + k-NN. The current framework belongs

to the application of neural network algorithms for working conditions, i.e., the health states from different pressure conditions are not invariant in nature with respect to the applied load and speed. Consequently, invariant fault diagnosis frameworks with transfer learning algorithms can be a fascinating direction for future studies. Moreover, this proposed algorithm makes use of CWTS grey image with a fixed resolution, which could be substituted with the scalogram image of adaptive resolution to better address the issues faced during the fault diagnosis of different mechanical faults due to the inconsistent working conditions of a centrifugal pump. Further, the proposed diagnostic framework can be extended to other relevant applications such as spherical tank, boiler tube, and pipeline fault diagnosis.

REFERENCES

[1] Y. Wang, C. Lu, H. Liu, and Y. Wang, "Fault diagnosis for centrifugal pumps based on complementary ensemble empirical mode decomposition, sample entropy and random forest," in *Proc. 12th World Congr. Intell. Control Autom. (WCICA)*, Jun. 2016, pp. 1317–1320.

[2] W. Zhao, Z. Wang, C. Lu, J. Ma, and L. Li, "Fault diagnosis for centrifugal pumps using deep learning and softmax regression," in *Proc. 12th World Congr. Intell. Control Autom. (WCICA)*, Jun. 2016, pp. 165–169.

[3] A. Rai and S. H. Upadhyay, "A review on signal processing techniques utilized in the fault diagnosis of rolling element bearings," *Tribol. Int.*, vol. 96, pp. 289–306, Apr. 2016.

[4] M. Sohaib and J.-M. Kim, "Fault diagnosis of rotary machine bearings under inconsistent working conditions," *IEEE Trans. Instrum. Meas.*, vol. 69, no. 6, pp. 3334–3347, Jun. 2020.

[5] M. Kang, M. R. Islam, J. Kim, J.-M. Kim, and M. Pecht, "A hybrid feature selection scheme for reducing diagnostic performance deterioration caused by outliers in data-driven diagnostics," *IEEE Trans. Ind. Electron.*, vol. 63, no. 5, pp. 3299–3310, May 2016, doi: 10.1109/TIE.2016.2527623.

[6] M. J. Hasan, M. Sohaib, and J.-M. Kim, "A multitask-aided transfer learning-based diagnostic framework for bearings under inconsistent working conditions," *Sensors*, vol. 20, no. 24, p. 7205, Dec. 2020.

[7] V. Muralidharan and V. Sugumaran, "Feature extraction using wavelets and classification through decision tree algorithm for fault diagnosis of mono-block centrifugal pump," *Measurement*, vol. 46, no. 1, pp. 353–359, Jan. 2013.

[8] H. Oh, J. H. Jung, B. C. Jeon, and B. D. Youn, "Scalable and unsupervised feature engineering using vibration-imaging and deep learning for rotor system diagnosis," *IEEE Trans. Ind. Electron.*, vol. 65, no. 4, pp. 3539–3549, Apr. 2018.

[9] N. R. Sakthivel, B. B. Nair, M. Elangovan, V. Sugumaran, and S. Saravanmurugan, "Comparison of dimensionality reduction techniques for the fault diagnosis of mono block centrifugal pump using vibration signals," *Eng. Sci. Technol., Int. J.*, vol. 17, no. 1, pp. 30–38, Mar. 2014.

[10] H. Zheng, R. Wang, Y. Yang, Y. Li, and M. Xu, "Intelligent fault identification based on multisource domain generalization towards actual diagnosis scenario," *IEEE Trans. Ind. Electron.*, vol. 67, no. 2, pp. 1293–1304, Feb. 2020.

[11] P. J. Unsworth, F. M. Discenzo, and V. S. Babu, "Detection of pump cavitation/blockage and seal failure via current signature analysis," U.S. Patent 2004/0 199 480, Oct. 7, 2004.

[12] S. Farokhzad, H. Ahmadi, and A. Jafary, "Fault classification of centrifugal water pump based on decision tree and regression model," *J. Sci. Today's World*, vol. 2, no. 2, pp. 170–176, 2013.

[13] H. Sun, S. Yuan, and Y. Luo, "Cyclic spectral analysis of vibration signals for centrifugal pump fault characterization," *IEEE Sensors J.*, vol. 18, no. 7, pp. 2925–2933, Apr. 2018.

[14] Z. Zheng and G. Xin, "Fault feature extraction of hydraulic pumps based on symplectic geometry mode decomposition and power spectral entropy," *Entropy*, vol. 21, no. 5, p. 476, May 2019.

[15] Y. Yang, H. Zheng, J. Yin, M. Xu, and Y. Chen, "Refined composite multivariate multiscale symbolic dynamic entropy and its application to fault diagnosis of rotating machine," *Measurement*, vol. 151, Feb. 2020, Art. no. 107233.

[16] G. Qiu, S. Huang, and Y. Gu, "Experimental investigation and multi-conditions identification method of centrifugal pump using Fisher discriminant ratio and support vector machine," *Adv. Mech. Eng.*, vol. 11, no. 9, 2019, Art. no. 1687814019878041.

[17] S. Farokhzad, H. Ahmadi, A. Jaefari, M. R. A. A. Abad, and M. R. Kohan, "Artificial neural network based classification of faults in centrifugal water pump," *J. Vibroeng.*, vol. 14, no. 4, pp. 1–11, 2012.

[18] H. Wang and P. Chen, "Intelligent diagnosis method for a centrifugal pump using features of vibration signals," *Neural Comput. Appl.*, vol. 18, no. 4, pp. 397–405, May 2009.

[19] M. A. S. Altobi, G. Bevan, P. Wallace, D. Harrison, and K. P. Ramachandran, "Fault diagnosis of a centrifugal pump using MLP-GABP and SVM with CWT," *Eng. Sci. Technol., Int. J.*, vol. 22, no. 3, pp. 854–861, Jun. 2019.

[20] S. Li, H. Wang, L. Song, P. Wang, L. Cui, and T. Lin, "An adaptive data fusion strategy for fault diagnosis based on the convolutional neural network," *Measurement*, vol. 165, Dec. 2020, Art. no. 108122.

[21] L. Gou, H. Li, H. Zheng, H. Li, and X. Pei, "Aeroengine control system sensor fault diagnosis based on CWT and CNN," *Math. Problems Eng.*, vol. 2020, Jan. 2020, Art. no. 5357146.

[22] U. Saeed, Y. D. Lee, S. U. Jan, and I. Koo, "CAFD: Context-aware fault diagnostic scheme towards sensor faults utilizing machine learning," *Sensors*, vol. 21, no. 2, p. 617, 2021, doi: 10.3390/s21020617.

[23] Z. Ahmad, A. E. Prosvirin, J. Kim, and J.-M. Kim, "Multistage centrifugal pump fault diagnosis by selecting fault characteristic modes of vibration and using Pearson linear discriminant analysis," *IEEE Access*, vol. 8, pp. 223030–223040, 2020, doi: 10.1109/ACCESS.2020.3044195.

[24] D. Li, G. Hu, and C. J. Spanos, "A data-driven strategy for detection and diagnosis of building chiller faults using linear discriminant analysis," *Energy Buildings*, vol. 128, pp. 519–529, Sep. 2016.

[25] Y. Jiang, S. Yin, and O. Kaynak, "Performance supervised plant-wide process monitoring in industry 4.0: A roadmap," *IEEE Open J. Ind. Electron. Soc.*, vol. 2, pp. 21–35, 2021.

[26] Z. Wang, H. He, Z. Wan, and Y. Sun, "Coordinated topology attacks in smart grid using deep reinforcement learning," *IEEE Trans. Ind. Informat.*, vol. 17, no. 2, pp. 1407–1415, Feb. 2021.

[27] Y. LeCun. (2015). *LeNet-5, Convolutional Neural Networks*. [Online]. Available: http//yann.lecun.com/exdb/lenet

[28] X. Yan and M. Jia, "A novel optimized SVM classification algorithm with multi-domain feature and its application to fault diagnosis of rolling bearing," *Neurocomputing*, vol. 313, pp. 47–64, Nov. 2018.

[29] J. Wang, Z. Mo, H. Zhang, and Q. Miao, "A deep learning method for bearing fault diagnosis based on time-frequency image," *IEEE Access*, vol. 7, pp. 42373–42383, 2019.

[30] S. Guo, T. Yang, W. Gao, C. Zhang, and Y. Zhang, "An intelligent fault diagnosis method for bearings with variable rotating speed based on pythagorean spatial pyramid pooling CNN," *Sensors*, vol. 18, no. 11, p. 3857, Nov. 2018.

[31] Z. YanPing, H. ShuHong, H. JingHong, S. Tao, and L. Wei, "Continuous wavelet grey moment approach for vibration analysis of rotating machinery," *Mech. Syst. Signal Process.*, vol. 20, no. 5, pp. 1202–1220, Jul. 2006.

[32] Ö. Türk and M. S. Özerdem, "Epilepsy detection by using scalogram based convolutional neural network from EEG signals," *Brain Sci.*, vol. 9, no. 5, p. 115, May 2019.

[33] S. Lapins, D. C. Roman, J. Rougier, S. De Angelis, K. V. Cashman, and J.-M. Kendall, "An examination of the continuous wavelet transform for volcano-seismic spectral analysis," *J. Volcanol. Geothermal Res.*, vol. 389, Jan. 2020, Art. no. 106728.

[34] Y. LeCun, L. D. Jackel, L. Bottou, C. Cortes, J. S. Denker, H. Drucker, I. Guyon, U. A. Müller, E. Säckinger, P. Simard, and V. Vapnik, "Learning algorithms for classification: A comparison on handwritten digit recognition," *Neural Netw., Stat. Mech. Perspective*, vol. 261, vol. 276, p. 2, 1995.

[35] Y. LeCun, Y. Bengio, and G. Hinton, "Deep learning," *Nature*, vol. 521, no. 7553, pp. 436–444, May 2015, doi: 10.1038/nature14539.

[36] N. Srivastava, G. Hinton, A. Krizhevsky, I. Sutskever, and R. Salakhutdinov, "Dropout: A simple way to prevent neural networks from overfitting," *J. Mach. Learn. Res.*, vol. 15, no. 1, pp. 1929–1958, 2014.

[37] S. Ioffe and C. Szegedy, "Batch normalization: Accelerating deep network training by reducing internal covariate shift," 2015, *arXiv:1502.03167*. [Online]. Available: http://arxiv.org/abs/1502.03167

[38] G. E. Dahl, T. N. Sainath, and G. E. Hinton, "Improving deep neural networks for LVCSR using rectified linear units and dropout," in *Proc. IEEE Int. Conf. Acoust., Speech Signal Process.*, May 2013, pp. 8609–8613.

[39] M. J. Hasan, M. M. M. Islam, and J.-M. Kim, "Acoustic spectral imaging and transfer learning for reliable bearing fault diagnosis under variable speed conditions," *Measurement*, vol. 138, pp. 620–631, May 2019, doi: 10.1016/j.measurement.2019.02.075.

[40] H. Wang, J. Xu, R. Yan, and R. X. Gao, "A new intelligent bearing fault diagnosis method using SDP representation and SE-CNN," *IEEE Trans. Instrum. Meas.*, vol. 69, no. 5, pp. 2377–2389, May 2020.

[41] L. Jing, M. Zhao, P. Li, and X. Xu, "A convolutional neural network based feature learning and fault diagnosis method for the condition monitoring of gearbox," *Measurement*, vol. 111, pp. 1–10, Dec. 2017.

[42] J. Ma, F. Wu, J. Zhu, D. Xu, and D. Kong, "A pre-trained convolutional neural network based method for thyroid nodule diagnosis," *Ultrasonics*, vol. 73, pp. 221–230, Jan. 2017.

[43] V. Thakkar, S. Tewary, and C. Chakraborty, "Batch normalization in convolutional neural networks—A comparative study with CIFAR-10 data," in *Proc. 5th Int. Conf. Emerg. Appl. Inf. Technol.*, Jan. 2018, pp. 1–5.

[44] *PMT-4008*, Wilo, Dortmund, Germany, 2020.

[45] *NI 9234*, Nat. Instrum., Austin, TX, USA, 2020.

[46] D.-T. Hoang and H.-J. Kang, "Rolling element bearing fault diagnosis using convolutional neural network and vibration image," *Cognit. Syst. Res.*, vol. 53, pp. 42–50, Jan. 2019.

[47] M. Sohaib and J.-M. Kim, "A robust deep learning based fault diagnosis of rotary machine bearings," *Adv. Sci. Lett.*, vol. 23, no. 12, pp. 12797–12801, Dec. 2017.

[48] M. Zhao, M. Kang, B. Tang, and M. Pecht, "Deep residual networks with dynamically weighted wavelet coefficients for fault diagnosis of planetary gearboxes," *IEEE Trans. Ind. Electron.*, vol. 65, no. 5, pp. 4290–4300, May 2018, doi: 10.1109/TIE.2017.2762639.

[49] M. Misiti, Y. Misiti, G. Oppenheim, and J.-M. Poggi, *Wavelets and Their Applications*. Hoboken, NJ, USA: Wiley, 2013.

[50] Y. Falamarzi, N. Palizdan, Y. F. Huang, and T. S. Lee, "Estimating evapotranspiration from temperature and wind speed data using artificial and wavelet neural networks (WNNs)," *Agricult. Water Manage.*, vol. 140, pp. 26–36, Jul. 2014.

[51] R. Bala and K. M. Braun, "Color-to-grayscale conversion to maintain discriminability," *Proc. SPIE*, vol. 5293, pp. 196–202, Dec. 2003.

[52] D. P. Kingma and J. Ba, "Adam: A method for stochastic optimization," 2014, *arXiv:1412.6980*. [Online]. Available: http://arxiv.org/abs/1412.6980

[53] C. Goutte and E. Gaussier, "A probabilistic interpretation of precision, recall and *F*-score, with implication for evaluation," in *Proc. Eur. Conf. Inf. Retr.*, 2005, pp. 345–359.

[54] P. Flach and M. Kull, "Precision-recall-gain curves: PR analysis done right," in *Proc. Adv. Neural Inf. Process. Syst.*, 2015, pp. 838–846.

[55] A. Luque, A. Carrasco, A. Martín, and A. de las Heras, "The impact of class imbalance in classification performance metrics based on the binary confusion matrix," *Pattern Recognit.*, vol. 91, pp. 216–231, Jul. 2019.

[56] L. van der Maaten and G. Hinton, "Visualizing data using t-SNE," *J. Mach. Learn. Res.*, vol. 9, pp. 2579–2605, Nov. 2008.

[57] Z. Ahmad, A. Rai, A. S. Maliuk, and J.-M. Kim, "Discriminant feature extraction for centrifugal pump fault diagnosis," *IEEE Access*, vol. 8, pp. 165512–165528, 2020.

[58] Q. Hu, E. F. Ohata, F. H. S. Silva, G. L. B. Ramalho, T. Han, and P. P. R. Filho, "A new online approach for classification of pumps vibration patterns based on intelligent IoT system," *Measurement*, vol. 151, Feb. 2020, Art. no. 107138.

[59] M. Sokolova and G. Lapalme, "A systematic analysis of performance measures for classification tasks," *Inf. Process. Manage.*, vol. 45, no. 4, pp. 427–437, Jul. 2009.

worked on the development of advanced algorithms for explainable condition monitoring system. His research interests include the data-driven fault diagnosis and anomaly detection of complex engineering systems using explainable artificial intelligence, machine learning, advanced signal processing, fault feature extraction, and feature engineering.

Mr. Hasan received the "Best Researcher Award" for three consecutive years for his outstanding contribution toward the research community from UOU. His recent awards and honors include the National Research Foundation (NRF) of Korea Research Fellowship Scholarship and the Brain Korea Scholarship for pursuing his Ph.D. Program.

AKHAND RAI received the B.Tech. degree in mechanical engineering from the College of Engineering Roorkee, Roorkee, India, in 2010, the M.Tech. degree in mechanical engineering from the Indian Institute of Technology (Banaras Hindu University), Varanasi, India, in 2012, and the Ph.D. degree in mechanical engineering from the Indian Institute of Technology (IIT) Roorkee, Roorkee, in 2018. He worked as a Postdoctoral Professional Researcher with the School of Electrical, Electronics and Computer Engineering, University of Ulsan, Ulsan, South Korea. He is currently working as an Assistant Professor with the School of Engineering and Applied Sciences, Ahmedabad University, India. His primary research interests include fault diagnosis and prognosis of rotating machines.
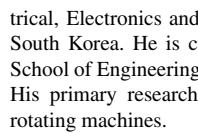
ZAHOOR AHMAD received the B.S. degree in computer engineering from the COMSATS Institute of Information Technology (CIIT), currently COMSATS University Islamabad (CUI), Attock, Pakistan, in 2016, and the M.S. degree in electronics and information engineering from Korea Aerospace University (KAU), Goyang, South Korea. He is currently pursuing the Ph.D. degree in computer engineering with the University of Ulsan, South Korea.

He has been a Graduate Research Assistant with the Smart HSE (Health, Safety, and Environment) Laboratory, University of Ulsan, since 2019. He worked on the development of advance algorithms for UAVs path planning. His current research interests include artificial intelligence, signal processing, fault diagnosis, vibration-based condition monitoring of industrial machinery, and fault feature extraction.

Mr. Ahmad received the institutional highest prize Gold Medal in B.S. from CUI. He was awarded with a fully funded scholarship for his M.S. degree from Korean Government project. His recent awards and honors include the National Research Foundation (NRF) of Korea Research Fellowship Scholarship and the University of Ulsan President Excellence Scholarship for pursuing his Ph.D. Program.

MD JUNAYED HASAN received the B.Sc. degree in computer engineering from Bangladesh Rural Advancement Committee University (BRACU), Dhaka, Bangladesh, in 2016. He is currently pursuing the Ph.D. degree in computer engineering with the University of Ulsan (UOU), Ulsan, Republic of Korea.

Since 2017, he has been working as a Graduate Research Assistant with the Ulsan Industrial Artificial Intelligence (UIAI) Laboratory, Department of Electrical, Electronics, and Computer Engineering, UOU, where he

JONG-MYON KIM (Member, IEEE) received the B.S. degree in electrical engineering from Myongji University, Yongin, South Korea, in 1995, the M.S. degree in electrical and computer engineering from the University of Florida, Gainesville, FL, USA, in 2000, and the Ph.D. degree in electrical and computer engineering from the Georgia Institute of Technology, Atlanta, GA, USA, in 2005.

He is currently a Professor with the School of IT Convergence, University of Ulsan, Ulsan, South Korea. His research interests include fault diagnosis and condition monitoring, multimedia-specific processor architecture, parallel processing, and embedded systems.

Dr. Kim is a member of the IEEE Industrial Electronics Society.

● ● ●